

Comparison of the Microstructure and Superconducting Properties of Eu–Ba–Cu–O and Gd–Ba–Cu–O Single Grain Samples

Tayebeh Mousavi, Yunhua Shi, John Durrell, Chris Grovenor, Susannah Speller

Abstract— Bulk Rare Earth–Ba–Cuprate [(RE)BCO] superconductors fabricated in the form of large single grains consisting of a $\text{REBa}_2\text{Cu}_3\text{O}_{7-\delta}$ (RE-123) matrix and $\text{RE}_2\text{BaCuO}_5$ (RE-211) inclusions can generate trapped magnetic fields that are up to ten times higher than the maximum fields obtainable in conventional Fe-based permanent magnets.

The choice of the Rare Earth (RE) element plays a key role in determining the growth rate of single grains, the precise microstructure, mechanical properties and hence the final superconducting properties of the bulk samples, and also the likelihood of RE substitution onto the Ba site which can degrade the performance.

In this work, we have studied the growth and microstructure of (RE)BCO single grains with RE = Gd and Eu, where the degree of Ba substitution is known to be very different. We have carried out detailed microstructural characterization of the phase distribution and composition using high resolution electron microscopy to understand the effects of Gd and Eu on the uniformity of the samples, the distribution of the secondary 211 phase, porosity and chemical variations in different regions of the melt-grown single grains.

Index Terms— Bulk Superconductor, REBCO, Microstructure, Single Grain

I. INTRODUCTION

Single grain RE–Ba–Cu–O [(RE)BCO] bulk superconductors are attractive for engineering applications due to their high trapped magnetic fields [1–2]. The trapped field of (RE)BCO bulks depends on the critical current density (J_c) which in turn depends on microstructure especially the presence of nanoscale defects and inclusions as flux pinning sites and the absence of high angle grain boundaries in the single grains [2]. High angle grain boundaries act as physical barrier to the flow of superconducting current and significantly decrease the macroscopic critical current density [3]. Therefore, it is essential that the bulk superconductors are fabricated in the form of single grains (or quasi single crystals) to generate large critical current densities and, subsequently, large magnetic fields [3].

In addition to the processing conditions (eg heat treatment steps) which considerably influence the microstructure of the REBCO bulks, the Rare Earth element also plays a key role in determining the growth rate and microstructure [2,3]. A number of rare earths including Nd, Sm, Eu, Gd, Dy and Y have been incorporated into (RE)BCO single grains, and the superconducting properties of the bulks carefully studied, and it is known that the final microstructure varies with the RE element [2–4]. This is because the peritectic temperature of REBCO and RE solubility in Ba–Cu–O melt vary for different Rare Earth elements leading to different growth conditions for the REBCO phase. This could considerably influences the microstructures of the REBCO bulks and the final superconducting properties, including the trapped magnetic fields [4].

Among all the REBCO compounds, YBCO is one of the most widely studied, and the properties can be further improved by doping and the use of mixed rare earth elements. Studies also show that compared to YBCO, the compounds of GdBCO, EuBCO and SmBCO can have higher critical current density at 77 K under self-field conditions [4,5] which is highly beneficial for engineering applications. However, the growth process requires optimization for each rare earth element.

We compare here the processing of GdBCO and EuBCO, two promising REBCO superconductors, in the form of large single grains. The focus is mainly on characterizing the microstructure of these bulks to understand how the choice of RE element (Gd and Eu) influences the growth, microstructure and final superconducting properties of these REBCO bulks. Both microstructure and composition has been analysed along the a axis of the single grain samples using scanning electron microscopy (SEM) and energy dispersive X-ray spectroscopy (EDX). This has enabled us to investigate the microstructure especially the particle size and distribution of the RE-211 phase, other possible phases, porosity and cracks.

II. EXPERIMENTAL METHODS

A. Melt-processing of GdBCO and EuBCO single grains

The growth process of single grains and sample preparation can be found in details in [5].

For the GdBCO sample, the raw powders of Gd-123 and Gd-211 were used (sourced from Toshima, 99.9% purity) with

T. Mousavi, C. Grovenor, and S. Speller are with the Department of Materials, University of Oxford, 16 Parks rd, Oxford OX1 3PH, U. K. (e-mail: tayebeh.mousavi@materials.ox.ac.uk; chris.grovenor@materials.ox.ac.uk;

susannah.speller@materials.ox.ac.uk), Yunhua Shi and John Durrell are with the Engineering Department, University of Cambridge, Trumpington Street, Cambridge, CB2 1PZ, U. K.

a precursor composition of [75 wt% $\text{GdBa}_2\text{Cu}_3\text{O}_{7-\delta}$ (Gd-123) + 25 wt% $\text{Gd}_2\text{BaCuO}_5$ (Gd-211)] + 0.5 wt% CeO_2 + 1.0 wt% BaO_2 + 10 wt% Ag_2O .

For the EuBCO sample, the raw powders of Eu-123 and Eu-211 were used (sourced from CAN superconductor, 99.9% purity) with a precursor composition of [75 wt% $\text{EuBa}_2\text{Cu}_3\text{O}_{7-\delta}$ (Eu-123) + 25 wt% $\text{Eu}_2\text{BaCuO}_5$ (Eu-211)] + 0.5 wt% CeO_2 + 1.5 wt% BaO_2 + 10 wt% Ag_2O .

B. Characterization

The phase analysis and microstructure of the GdBCO and EuBCO single grains were characterized by means of X-ray diffraction (XRD) and scanning electron microscopy (SEM). The XRD was performed in a Panalytical Empyrean radiation instrument using $\text{Cu K}\alpha$ radiation. The XRD measurements covered an angular 2θ range from 30° to 130° using a scanning step of 0.01° and a scanning speed of 1° min^{-1} .

The microstructure of the samples was characterized by scanning electron microscopy (SEM-Zeiss EVO MA10, and Zeiss Merlin), and compositional analysis was carried out by Energy Dispersive X-ray analysis (EDX) using an Oxford Instruments X-Max 150 silicon drift detector.

The trapped fields of the single grains were measured by a scanning Hall probe technique in a zero-field-cooled magnetization process and at a distance of 0.5 mm from the sample surface.

III. RESULTS

A. Phase analysis

The XRD patterns of GdBCO and EuBCO samples are shown in Figure 1. Both XRD patterns include sharp and strong peaks (indicated by \bullet) corresponding to the orthorhombic structure of the RE-123 phase. The presence of only (00 l) diffraction peaks confirms that the bulks are single grains with their (00 l) planes parallel to the top surface. In addition to the RE-123 diffraction peaks, there are small peaks (indicated by $*$) corresponding to RE-211 grains showing no preferred orientation.

The XRD data also shows that the GdBCO diffraction peaks are slightly shifted towards higher angles compared to those of EuBCO due to the larger lattice parameters of EuBCO because the atomic radius of Eu (240 pm) is larger than Gd (180 pm).

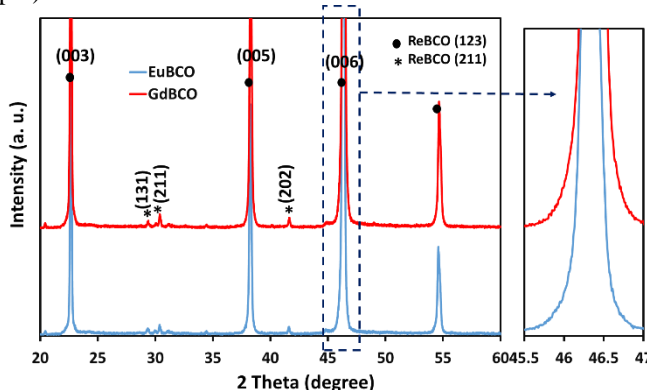


Figure 1. XRD patterns of the EuBCO and GdBCO single grains.

B. Phase distributions

The final performance of the ReBCO bulks is determined by their maximum trapped field which is defined by the critical current density dependent on the flux pinning sites and microstructure. It is believed that flux pinning in these samples is primarily from the RE-211 phase [6-8]. A large J_C may be achieved by the presence of an optimum volume fraction, size and distribution of RE-211 second phase material in the superconducting RE-123 phase matrix [6].

Significantly, for a given volume fraction, a fine particle size of the RE-211 phase can increase J_C due both to an increasing number of pinning sites and to the defect size becoming a better match to the flux vortex core size [2,6]. To investigate the particle size and distribution of the RE-211 phase in our GdBCO and EuBCO samples, SEM images were taken systematically along the a axis. Figure 2a and b show typical distributions of the RE-211 phase (round light grey features) in the RE-123 matrix (dark grey) in EuBCO and GdBCO samples respectively. The average particle size of the RE-211 phase was calculated from these SEM images using ImageJ software. Figure 2c shows the average particle size of the RE-211 phase along the a growth direction at different distances from the centre of the sample. Each data point in Figure 2c is collected from a region of $50 \mu\text{m} \times 50 \mu\text{m}$. It can be seen that for both samples the RE-211 particle size becomes smaller with increasing distance from the centre. For example, the average particle size of the Gd-211 phase is about $2.7 \mu\text{m}$ close to the centre, and it reduces to $1.85 \mu\text{m}$ 5 mm along a axis (ie. close to the edge). This trend has also been seen in ReBCO bulks and can be explained by the particle pushing/trapping theory [9-10].

Figure 2c also shows that the average 211 particle size is slightly smaller for the GdBCO sample compared to the EuBCO at all positions. Figure 2d shows the volume fraction of the RE-211 phase along the a -axis. Each data point in this graph has been calculated from a $50 \mu\text{m} \times 50 \mu\text{m}$ area using ImageJ software. The area fraction occupied by the RE-211 phase increases along the a -axis for both GdBCO and EuBCO samples, however, the GdBCO sample shows less variations in the volume fraction of the Gd-211 phase along the a -axis. It can be concluded that the RE-211 particles increase in volume fraction but decrease in average size along the a -axis. Although this trend was observed for both samples, the GdBCO bulk consists of smaller Gd-211 particles with more uniform distribution of Gd-211 particles compared to the Eu-211 particles in the EuBCO bulk.

In addition to the RE-211 phase, small square features (shown in Figure 3a and b) were also found in both samples. The elemental maps of these features (presented in Figure 3c) revealed that these features are BaO_2 . EDX line scan was also carried out over these features and the results confirmed the presence of BaO_2 in both samples (Figure 3d).

The BaO_2 particles were intentionally added to the initial precursor powder in order to suppress the Gd/Ba substitution and the formation of solid solution between RE and Ba.

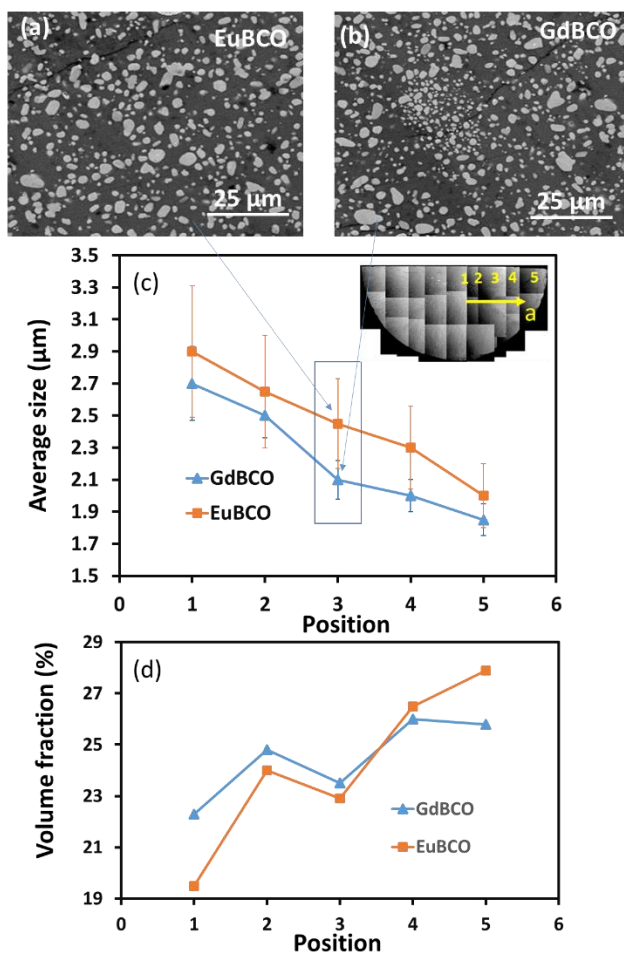


Figure 2. (a) and (b) Back-scattered SEM images of the EuBCO and GdBCO bulks respectively, (c) and (d) the average particle size and volume fraction of the RE-211 phase along the a direction for EuBCO and GdBCO single grains. The inset in (c) shows the position of each data point from the centre (number 1, 2mm far from the centre) to the edge (number 5, 10 mm far from the centre) along the a-axis.

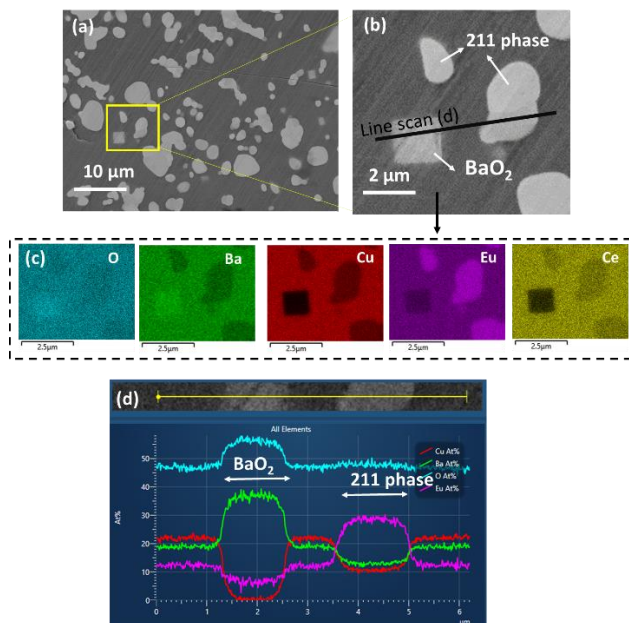


Figure 3. (a and b) Back-scattered SEM image of the EuBCO bulk, (c) Elemental maps of the selected region showing the presence of BaO₂ particles, (d) EDX line scan over the selected features in (b).

C. Ag particles, cracks and porosity

Ag can be introduced to the REBCO single grain microstructure to improve mechanical properties [2]. Figure 4 shows the SEM image of the EuBCO bulk along with the elemental maps which exhibit the presence of individual Ag particles distributed throughout the Eu-123 matrix. The light grey regions are Eu-211 particles, whereas the large bright regions, as indicated in Figure 4, are Ag particles as confirmed by EDX. The Ag particles are almost round.

In order to compare the particle size and distribution of the Ag particles in EuBCO and GdBCO samples, SEM images with the same magnifications were taken from various regions of both samples. Figure 5 shows some of these images at different magnifications. It can be seen that the Ag particles are dispersed in both samples, but the Ag particle size in EuBCO lies within 5-40 µm which is a much broader range compared to that in GdBCO (10-20 µm).

It was also found that the Ag particles are more evenly distributed in the GdBCO compared to the EuBCO. A possible hypothesis is that during the melt-processing, the Ag particles melt and the liquid silver fills the porosities available in the samples. As the particle size of the initial powders is much smaller for the GdBCO, it can be suggested that the porosity between powder particles are much smaller with a more uniform distribution in GdBCO sample compared to the EuBCO bulk. As a result, when the liquid silver penetrates into the porosities, they will be solidified in smaller particles size with higher uniformity in the GdBCO sample.

It is worth mentioning that only small number of cracks were found in these samples which can be due to the presence of Ag particles. It has been reported that the introduction of Ag results in the formation of significantly fewer cracks [11]. The reduction in crack formation is expected to reduce significantly the probability of catastrophic fracture of samples that may otherwise fail due to high internal magnetic pressure.

It was also found that the GdBCO sample contained fewer cracks and porosity compared to the EuBCO. A hypothesis in the literature regarding the formation of the cracks in REBCO samples is that the cracks are possibly formed during RE-123 the oxygenation process [11-14] where the tetragonal to orthorhombic transformation causes a volume change in the large single grains and possibly creates cracks [8-10]. In this case, the presence of fewer cracks in the GdBCO sample can be explained by the fact that during the high temperature sintering process, RE ions tend to substitute for Ba ions in the lattice site, and the smaller the RE ion radius the lower the resulting lattice strain (the Gd atoms are smaller than Eu) and likelihood of crack formation.

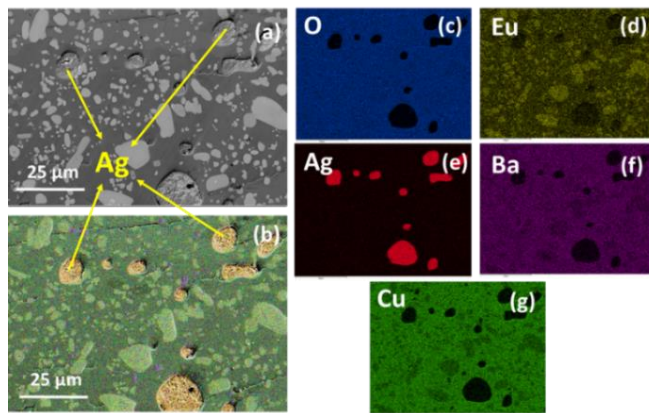


Figure 4. (a) Back-scattered SEM image of the EuBCO bulk, (b-g) elemental maps of region (a) showing the distribution of Ag particles in the microstructure.

D. Trapped field

The trapped magnetic field in these GdBCO and EuBCO superconducting bulks were measured at 77 K by field cooling process in an applied field of 1.4 T. The trapped field profiles are shown in Figure 6. As can be seen the trapped field is higher for the GdBCO bulk (0.54 T) compared to the EuBCO bulk (0.4 T). Since both samples are the same size, the difference in trapped field is related to both intrinsic superconducting properties of these samples and the microstructural features. The magnitude of the J_C is determined by the ability of the microstructure to pin magnetic flux, with a larger macroscopic J_C producing a larger trapped field [1,5]. Since J_C is correlated to the size and distribution of the RE-211 phase, the more uniform the distribution of 211 particles should result in a more uniform critical current values throughout the sample, and the higher the density of small 211 particles should increase the magnitude of the critical current. In this study the GdBCO sample has a more optimized microstructure for higher J_C values as it contains smaller RE-211 particles and less cracks and porosity. However, it should also be considered that the RE element, which plays a key role in the fundamental superconducting properties, is different in these two samples.

IV. CONCLUSION

We compare the microstructure and trapped field properties of 2 cm superconducting GdBCO and EuBCO single-grain bulks grown by melt-processing technique. It was observed that RE-211 secondary-phase particles are distributed homogeneously in both samples in a RE-123 superconducting matrix. The employment of fine starting Gd-211 powders led to a reduction in the mean diameter of Gd-211 particles dispersed in the bulk. The Ag particles are smaller and more uniform in the GdBCO leading to fewer cracks in this sample. Both these features explain why the GdBCO shows higher trapped field compared to the EuBCO sample, and suggest processing improvements that can be used to further improve the performance of these materials.

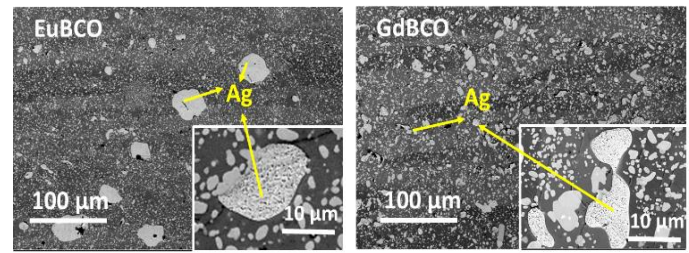


Figure 5. Back-scattered SEM images of the GdBCO and EuBCO bulks showing the different scale of the Ag particles.

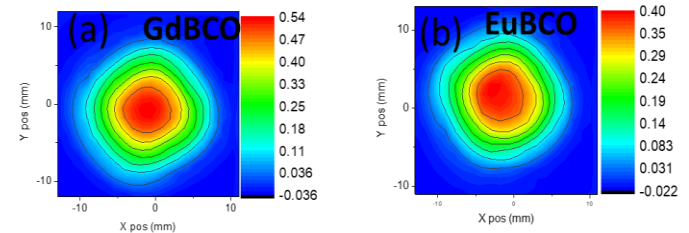


Figure 6. Trapped magnetic field profile of the (a) GdBCO and (b) EuBCO superconducting bulks measured at 77 K.

REFERENCES

- [1] D. Dimos et al, Superconducting transport properties of grain boundaries in $\text{YBa}_2\text{Cu}_3\text{O}_7$ bicrystals *Phys. Rev. B* 41 4038–49, 1990.
- [2] D. Namburi et al, The processing and properties of bulk (Re)BCO superconductors, *Supercond. Sci. Technol.* 34 053002, 2021.
- [3] J. Durrell, Importance of low-angle grain boundaries in $\text{YBa}_2\text{Cu}_3\text{O}_{7-\delta}$ coated conductors *Supercond. Sci. Technol.* 22 013001, 2009.
- [4] S. Zhang et al Broad temperature study of RE-substitution effects on critical current behavior of REBCO superconducting tapes *Supercond. Sci. Technol.* 31 125006, 2018.
- [5] Y. Shi et al, The growth and superconducting properties of REBCO single grains with combined RE elements, *Supercond. Sci. Technol.* 33 035003, 2020.
- [6] H. Babu et al, Artificial flux pinning centers in large, single-grain (RE)BCO superconductors *Appl. Phys. Lett.* 83 4806–8, 2003.
- [7] S. Pavan Kumar Naik, N. Devendra Kumar, P. Missak Swarup Raju, T. Rajasekharan and V. Seshubai, "Effect of infiltration temperature on the properties of infiltration growth processed YBCO superconductor", *Physica C*, vol. 487, pp. 72-76, 2013.
- [8] T. Mousavi, C. Aksoy, C. Grovenor, "Phase evolution of superconducting Sn-In-Bi solder alloys", *IEEE Transaction on Applied superconductivity*, 26(3) 7800104, 2016
- [9] A. Endo et al, Macrosegregation of $\text{Y}_2\text{Ba}_1\text{Cu}_1\text{O}_5$ particles in $\text{Y}_1\text{Ba}_2\text{Cu}_3\text{O}_{7-\delta}$ crystals grown by an undercooling method *J. Mater. Res.* 11 795, 1996.
- [10] T. Mousavi, Z. Hong, A. Morrison, A. London, P.S. Grant, C. Grovenor, "A new approach to fabricate superconducting NbTi alloys", *Supercond. Sci. Technol.*, vol. 30 (9), pp. 094001, 2017.
- [11] S. Sabooni, T. Mousavi, F. Karimzadeh, "Thermodynamic analysis and characterization of nanostructured Cu(Mo) compounds prepared by mechanical alloying and subsequent sintering", *Powder Metallurgy* 55(3) 222-2227, 2012.
- [12] P. Diko, Cracking in melt-grown Re-Ba-Cu-O single grain bulk superconductors, *Supercond. Sci. Technol.* 17 R45, 2004.
- [13] T. Mousavi, C. Grovenor, S. Speller, "Characterization of superconducting $\text{Fe}(\text{Se}_{1-x}\text{Te}_x)$ thin films deposited on MgO substrates by sputtering", *Journal of Materials Science* 50(21) 6970-6978, 2015.
- [14] N. Nariki, N. Sakai, M. Murakami and I. Hirabayashi, "High critical current density in Y-Ba-Cu-O bulk superconductors with very fine Y211 particles", *Supercond. Sci. Technol.*, vol. 17, pp. S30-S35, 2004.